

THE BI-VARIATE LUMINOSITY-COLOR DISTRIBUTION OF IRAS GALAXIES, AND IMPLICATIONS FOR THE HIGH REDSHIFT UNIVERSE

S. C. CHAPMAN,¹ G. HELOU,¹ G. F. LEWIS,² D. A. DALE³

California Institute of Technology, Pasadena, CA 91125, U.S.A.

Anglo-Australian Observatory, P.O. Box 296, Epping, NSW 1710, Australia

Department of Physics & Astronomy University of Wyoming Laramie, WY 82071

Draft version October 29, 2018

ABSTRACT

We present a characterization of the local luminosity-color, bi-variate distribution of IRAS galaxies from the 1.2 Jy sample, selected at 60 μ m. The $\mathcal{R}(60, 100)$ infrared color is used as the best single parameter description of the IR spectral energy distribution of galaxies. We derive an analytical form of the distribution and use it to constrain the effect of the IR color distribution on evolution models for high redshift, farIR luminous galaxies. Our adopted evolution retains the locally observed correlation between luminosity and color, such that the larger characteristic luminosities at higher redshift have a warmer characteristic color. The width of the color distribution at a given luminosity remains constant for all redshifts. We demonstrate that there is the potential for both hotter and colder sources to be missed in cosmological surveys. An evolving bi-variate luminosity function coupled with the cold source bias of sub-mm selected surveys suggests the existence of a large population of cold sources appearing in such surveys. Likewise, a hot source bias for most SIRTf wavebands together with a bi-variate model suggests an excess of hot sources being selected. We test the evolutionary form against available data for higher redshift, farIR galaxies. The data do not reveal evidence for any strong evolution in the characteristic luminosity-color distribution as a function of redshift over $0 < z < 1$. However, there is marginal evidence for a broadening of the color distribution at higher redshifts, consistent with our locally characterized trend of a broadening in the IR color distribution at the highest luminosities.

Subject headings: galaxies: evolution — galaxies: formation — sub-mm: galaxies — radio: galaxies — IR: galaxies

1. INTRODUCTION

The local infrared-luminous galaxies detected by the *IRAS* satellite exhibit a vast array of source properties. Infrared color has typically been used to attempt to parametrize the *IRAS* population (Soifer & Neugebauer 1991). Dale et al. (2001) demonstrated that the $S_{60\mu\text{m}}/S_{100\mu\text{m}}$ flux ratio or color (hereafter referred to as $\mathcal{R}(60, 100)$) provides the best single parameter characterization of the *IRAS* galaxy population, in addition to luminosity. While a complicated array of dust properties contribute to the spectral energy distribution (SED) of each galaxy, studies of *IRAS* galaxies have typically reduced the description to a best fit single dust temperature, T_d , with a one-to-one mapping to $\mathcal{R}(60, 100)$. Indeed, changing the dust temperature has been demonstrated to have a significantly larger effect on the galaxy SED than dust emissivity, mid-IR spectral index, or cosmology (Blain et al. 2002). The inferred luminosity of an infrared galaxy for a fixed observed mid-IR flux density increases by a factor of 10 if the dust temperature is doubled.

It has been demonstrated that low-redshift *IRAS* galaxies exhibit slowly varying correlations of $\mathcal{R}(60, 100)$ with luminosity (Dale et al. 2001; Dunne et al. 2000; Andreani & Franceschini 1996). However, over a large spread of luminosities the $\mathcal{R}(60, 100)$ ratio of infrared galaxies does change systematically. Fitting single dust temperature (T_d) models to $\mathcal{R}(60, 100)$, we find ~ 20 K for low-redshift spirals (Reach et al. 1995; Alton et al. 2000; Dunne & Eales 2001) and 30 K–60 K for the high luminosity objects typically detected by *IRAS* (Soifer & Neugebauer 1991, Stanford et al. 2000). High redshift, hyper-luminous galaxies can show dust temperatures of up to 110 K (e.g., Lewis et al. 1998), implying a continuation in the luminosity- T_d relation out to the higher luminosities char-

acteristic of the distant Universe.

However, while a statistical relation exists between the $\mathcal{R}(60, 100)$ and IR luminosity, the distribution is broad. We find in substantial numbers both extremely luminous, yet cold galaxies, as well as low luminosity, hot galaxies. One surprisingly cold and luminous galaxy, Arp 302 (or UGC 9618/NGC 5051), has been identified from the *IRAS* bright galaxy sample (BGS) with $S_{60\mu\text{m}}=6.8$ Jy, $S_{100\mu\text{m}}=15.3$ Jy, and $L_{\text{FIR}}=3.89 \times 10^{11} L_{\odot}$. This is the system with largest deviation from the median $\mathcal{R}(60, 100)$ for its luminosity. Lo, Gao & Guendl (1997) suggest this galaxy is the most massive known (in terms of CO gas mass). By contrast, galaxies with very hot IR color, and without obvious AGN contributions, have been identified from the faintest L_{FIR} sources detected by *IRAS*. NGC1377, NGC4491 and IRAS1953 with $\mathcal{R}(60, 100) \sim 1$ and $L_{\text{FIR}} \sim 10^9 L_{\odot}$ are as hot or hotter than the Ultra-Luminous Infrared Galaxy (ULIG), Arp220, but with 10^{-3} the FIR luminosity (Roussel et al. 2003).

The possible importance of cold, luminous galaxies to farIR and sub-mm surveys has been pointed out by Eales et al. (1999, 2000). This has recently been highlighted observationally by Chapman et al. (2002a) who demonstrated that cold and luminous sources exist at higher redshift, identifying two *ISO-FIRBACK* sources (FB1-40 and FB1-64) with $L_{\text{TIR}} > 10^{12} L_{\odot}$ with $z \lesssim 1$ galaxies, and finding best fit single temperature greybodies of 26 K and 31 K respectively (dust emissivity $\beta = 1.6$). The local cold source, Arp 302, approximately matches the color and luminosity of FB1-40. However, FB1-40 and FB1-64 were discovered from a random sampling of the sub-mm luminous FIRBACK sources, and they cannot be considered as an insignificant portion of the high- z ULIG population.

It is therefore a concern that studies of the evolving galaxy populations typically assume a small range of template galaxy spectral energy distributions (SEDs), sampling only the monotonic relation of dust temperature to luminosity in choosing the SED templates (Blain et al. 1999a,b, Malkan & Stecker 2000, Rowan-Robinson 2001, Chary & Elbaz 2001, Chapman et al. 2002b, Franceschini et al. 2002). Modeling efforts have in effect tied the dust temperature directly to the farIR luminosity, ignoring the T_d distribution for each luminosity class. This in part may be a result of the fact that the $\mathcal{R}(60, 100)$ distribution for local IRAS galaxies has never been carefully studied, and no analytical form for the distribution has been presented.

Importantly, an evolving distribution bi-variate in luminosity and color, $\Phi(\mathcal{L}, C)$, consistent with the broad distribution observed locally should subsume a non-negligible fraction of both cold, luminous galaxies and hot, faint galaxies. Surveys which select objects at either the cold Raleigh-Jeans tail of the dust SED, or the hot Wien tail, will preferentially detect appropriately cold or hot objects for a given luminosity class, if they exist in non-negligible numbers. For instance, the cold source bias of farIR (e.g., $170\mu\text{m}$) and submillimeter selected surveys will result in any existing population of cold sources being over-represented.

At the highest redshifts, the poorly understood submillimeter (sub-mm) population is thought to dominate the most luminous IR galaxies. Since the discovery of high redshift sub-mm sources (Smail, Ivison & Blain 1997), there has been an ongoing debate about their nature and their dust properties. In the absence of redshifts, it is difficult to understand whether they represent hot sources at very high redshifts, or colder sources at more modest redshifts (e.g. Eales et al. 1999, 2000), similar to FB1-40 and FB1-64 (Chapman et al. 2002a). Chapman et al. (2003a) have measured spectroscopic redshifts for radio identified sub-mm galaxies, claiming a typical dust temperature of $\sim 40\text{K}$ by assuming the empirical relation between the far-IR and radio observed locally (e.g., Helou et al., 1985). However, without additional SED measurements, it is unclear what distribution in dust properties for the sub-mm galaxies remains consistent with their currently measured properties.

In this paper, we characterize the local luminosity-color, bi-variate distribution, $\Phi(\mathcal{L}, C)$, of IRAS galaxies from the 1.2Jy sample, selected at $60\mu\text{m}$. We represent the infrared luminosity with L_{TIR} , and the $\mathcal{R}(60, 100)$ IR-color is used as the best single parameter description of the IR SED of galaxies. L_{TIR} is defined as in Dale et al. (2001), integrating over the SED from $3\text{--}1100\mu\text{m}$. These authors define a bolometric conversion between the more typical FIR luminosity (e.g., Helou et al., 1985) as

$$\log(\text{TIR}/\text{FIR}) = a_0 + a_1x + a_2x^2 + a_3x^3 + a_4x^4$$

where $x = \log \frac{f_\nu(60\mu\text{m})}{f_\nu(100\mu\text{m})}$ and $[a(z=0)] = [0.2738, -0.0282, 0.7281, 0.6208, 0.9118]$. The first part of the paper is directed at the derivation of an analytical form for the local IRAS color distribution. In order to constrain the effect of the IR color distribution on our understanding of high redshift farIR luminous galaxies, we evolve the bi-variate distribution according to luminosity evolution prescriptions used in the literature. For convenience, we use the terms ‘color’ (meaning 60/100 micron flux ratio) and ‘temperature’ interchangeably, even though we do not collapse the SED description to a single temperature blackbody. The color is taken to be a diagnostic of the typical heating conditions in the ISM of a galaxy, and therefore would be indicative of a characteristic dust temperature. Section 2 describes our sample used to construct $\Phi(\mathcal{L}, C)$. Section 3 pro-

vides a statistical analysis of the 1.2Jy sample, and provides a best fit analytical form to $\Phi(\mathcal{L}, C)$. Section 4 explores the evolutionary behavior of $\Phi(\mathcal{L}, C)$, while Section 5 compares the evolving $\Phi(\mathcal{L}, C)$ to existing data sets at higher redshift.

2. SAMPLE SELECTION

Our starting point for this study is the $S_{60\mu\text{m}} > 1.2\text{Jy}$ sample of galaxies (Fisher et al. 1995). We plot the $\mathcal{R}(60, 100)$ distribution of these galaxies as a function of both L_{FIR} and L_{TIR} in Fig. 1. L_{FIR} is calculated directly from the $60\mu\text{m}$ and $100\mu\text{m}$ flux densities and the redshift as described in Helou et al. (1985). The L_{TIR} parameter represents a bolometric correction for the flux from 3 to 1100 microns, and represents a larger correction for sources with cooler $\mathcal{R}(60, 100)$ colors, as seen in the comparison of the two panels of Fig. 1. The analytical expression mapping the average FIR luminosity to TIR luminosity from Dale et al. (2001) was reproduced in the previous section.

While studying this sample, we noticed a significant tail of very cold and luminous galaxies, departing bi-modally from the main distribution (see Fig. 1). Upon closer inspection of the 60 and $100\mu\text{m}$ IRAS fluxes using the XSCANPI application provided by the Infrared Processing and Analysis Center (IPAC), we found that almost 100% of these sources have spurious measurements. Firstly, the cirrus contamination can be large, affecting the $100\mu\text{m}$ more than $60\mu\text{m}$ and leading to an apparently small $60\mu\text{m}/100\mu\text{m}$ ratio. Secondly, the $60\mu\text{m}$ flux measurements found for some of the sources from XSCANPI were less than 1.2Jy, and should not be included in our catalog.

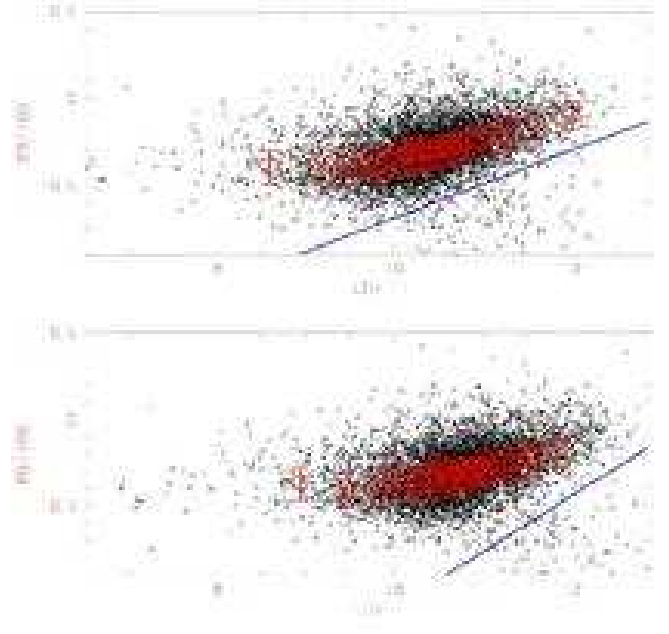


FIG. 1.— The L_{FIR} and L_{TIR} distributions in $\mathcal{R}(60, 100)$. Spurious cold, luminous sources have been removed from the sample, as indicated here by solid lines delimiting the region of spurious sources. The medians in equal number bins are plotted as large circles, with the interquartile range shown in error bars.

We flagged all such sources in our sample and removed them from subsequent consideration. To ensure that this effect did not significantly contaminate the main distribution, we randomly selected 200 of the sources with $L_{\text{FIR}} > 10^{11}$ for XSCANPI analysis, finding them to have correct flux estimates to within 5% of the Fisher et al. (1995) values. We then derive

the TIR luminosity function with the revised catalog of 1.2Jy sources. We adopt an accessible volume technique as described in (Avni & Bahcall 1980) Our general luminosity function is represented as

$$\Phi(L)\Delta L = \sum_i \frac{1}{V_i} \quad (1)$$

with $\Phi(L)\Delta L$ as the number density of sources (Mpc^{-3}) in the luminosity range L to $L + \Delta L$. The accessible volume, V_i , represents the i th source in the sample, the maximum volume in which the object could be located and still be detected in the *IRAS* 1.2Jy $60\mu\text{m}$ catalog. The sum is then over all sources within the luminosity range. We then map sources to their TIR luminosity using the above definition. Our constructed TIR luminosity function is therefore directly related to the $60\mu\text{m}$ luminosity function for this sample.

Figure 1 also shows the median $\mathcal{R}(60, 100)$ values and the interquartile range, revealing the dust temperature to luminosity relation. In the subsequent sections, we shall study and characterize this relation.

3. RESULTS

3.1. Statistics

In choosing a luminosity variable in $\Phi(\mathcal{L}, \mathcal{C})$ to describe the distribution of galaxies, it is desirable to minimize the dependencies between \mathcal{L} and \mathcal{C} . L_{TIR} has been shown to provide less dependency than L_{FIR} on IRAS colors (Dale et al. 2001). Similarly, $\mathcal{R}(60, 100)$ has been demonstrated to parametrize the variation in mid–farIR properties better than any other combination of IRAS bands (Dale et al. 2001).

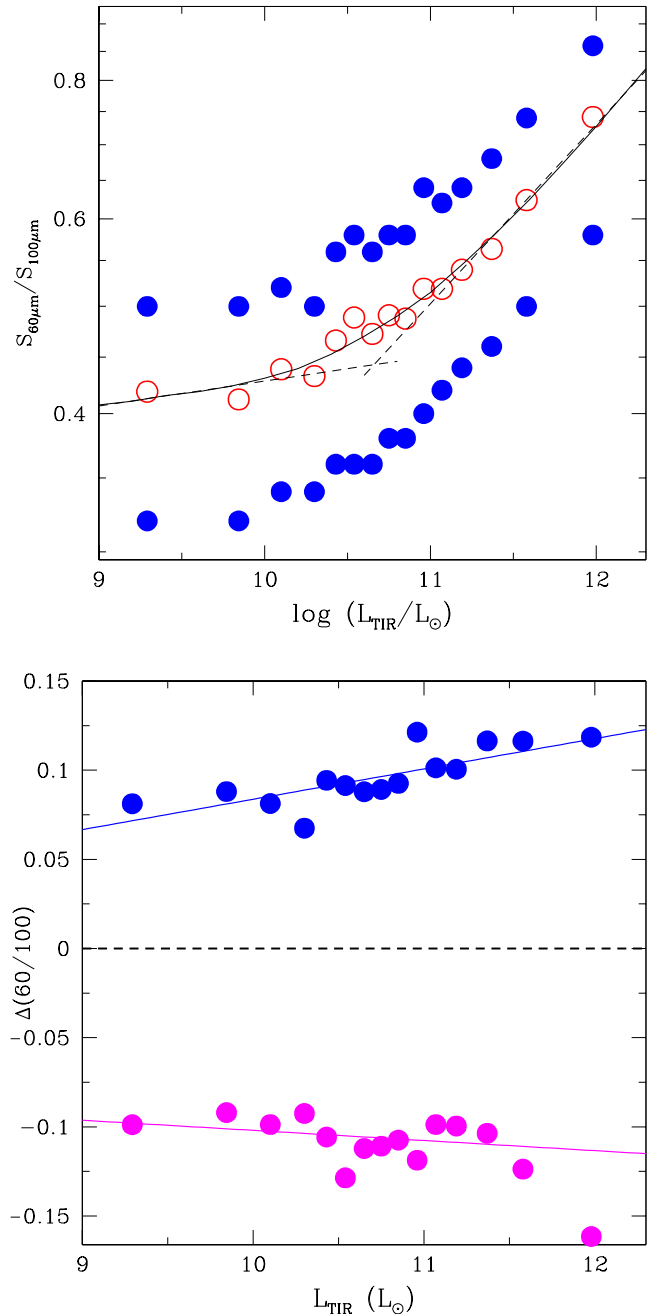


FIG. 2.— **Upper Panel:** The 1st quartile, median, and last quartile for the 1.2Jy sample with a log scaling in $\mathcal{R}(60, 100)$, suggesting a roughly constant width and shape in log space. **Lower Panel:** The same statistics with the median subtracted, shown in a linear scaling emphasizing the small linear increase in width with increasing luminosity. The width is constant in $\log(\mathcal{R}(60, 100))$.

Having chosen our variable representation of $\Phi(\mathcal{L}, \mathcal{C})$, we can proceed to quantify the relation for the $S_{60}>1.2\text{Jy}$ IRAS sample and explore the implications. We begin by calculating the median and first/last quartile statistics for the 1.2Jy sample, corrected for spurious cold, luminous sources as described in section 2. The analytic relation in the distribution median is well fit by a dual power law, as shown in figure 2:

$$\log \mathcal{R}(60/100) = 0.162 \times \log(L_{\text{TIR}}/L_{\odot}) - 2.080, \quad L_{\text{TIR}} > 5 \times 10^{10} L_{\odot}$$

$$\log \mathcal{R}(60/100) = 0.022 \times \log(L_{\text{TIR}}/L_{\odot}) - 0.593, \quad L_{\text{TIR}} < 5 \times 10^{10} L_{\odot}.$$

We express this composite function with a smooth transition

as:

$$\mathcal{R}(60/100) = C_* \times \left(1 + \frac{\mathcal{L}_*}{L_{\text{TIR}}}\right)^{-\delta} \times \left(1 + \frac{L_{\text{TIR}}}{\mathcal{L}_*}\right)^{\gamma}$$

$$\text{with, } \gamma = 0.16, \delta = 0.02, C_* = 0.45, \mathcal{L}_* = 5.0 \times 10^{10} L_{\odot}$$

The statistics and the fitted relation are shown in Fig. 2a. We also fit the width of the inter-quartile statistics after removing the median (Fig. 2b). The width of the distribution described in terms of this statistic is essentially constant in $\log(\mathcal{R}(60, 100))$ as a function of L_{TIR} , therefore showing a slight broadening in $\mathcal{R}(60, 100)$ as shown in Fig. 2b. At the highest luminosities there is some evidence for significant broadening of even the $\log(\mathcal{R}(60, 100))$, although the statistics are poor and there remains a concern that all spurious sources have not been removed from the sample (section 2).

These equations provide a simple, first order description of the $\Phi(\mathcal{L}, C)$ distribution of IRAS galaxies from which to gage a more comprehensive analysis. This expression should be suitable for many applications and evolutionary extrapolations.

3.2. Fitting the $\Phi(\mathcal{L}, C)$ distribution

We now consider the detailed distributions in $\mathcal{R}(60, 100)$ for the 1.2 Jy sample. Histograms of the distribution from each luminosity bin are plotted in Fig. 3. For clarity, a fixed constant is introduced to offset each class of L_{TIR} . With no apriori assumptions about the $\mathcal{R}(60, 100)$ distribution of the IRAS sources, we begin by testing whether the population might be well represented by a gaussian in the $\mathcal{R}(60, 100)$ color. A gaussian in both linear $\mathcal{R}(60, 100)$ and $\log \mathcal{R}(60, 100)$ was first fit to each bin of 380 sources. The functional form

$$C + B * x + D * \exp[-1/2 \times \left(\frac{x-A}{E}\right)^2],$$

where x represents $\mathcal{R}(60, 100)$, was fit to each histogram of 380 sources. An equal weighting of the points in the histogram was assumed in the fitting. The residuals were compared, with the χ^2 being a factor ~ 2 smaller for the gaussian in \log (or \log normal distribution), suggesting the log normal as the more appropriate representation.

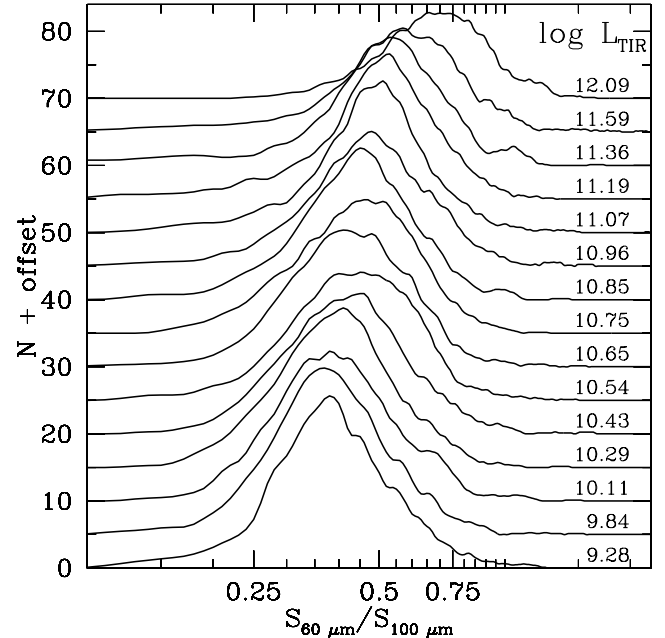


FIG. 3.— The $\Phi(\mathcal{L}, C)$ distribution in log IR-color, shown as a smoothed histogram. The effective histogram bin size is $d\mathcal{R}(60, 100)=0.05$. Histograms of L_{TIR} are shown offset by a fixed constant for clarity, and labeled on the right in L_{\odot} .

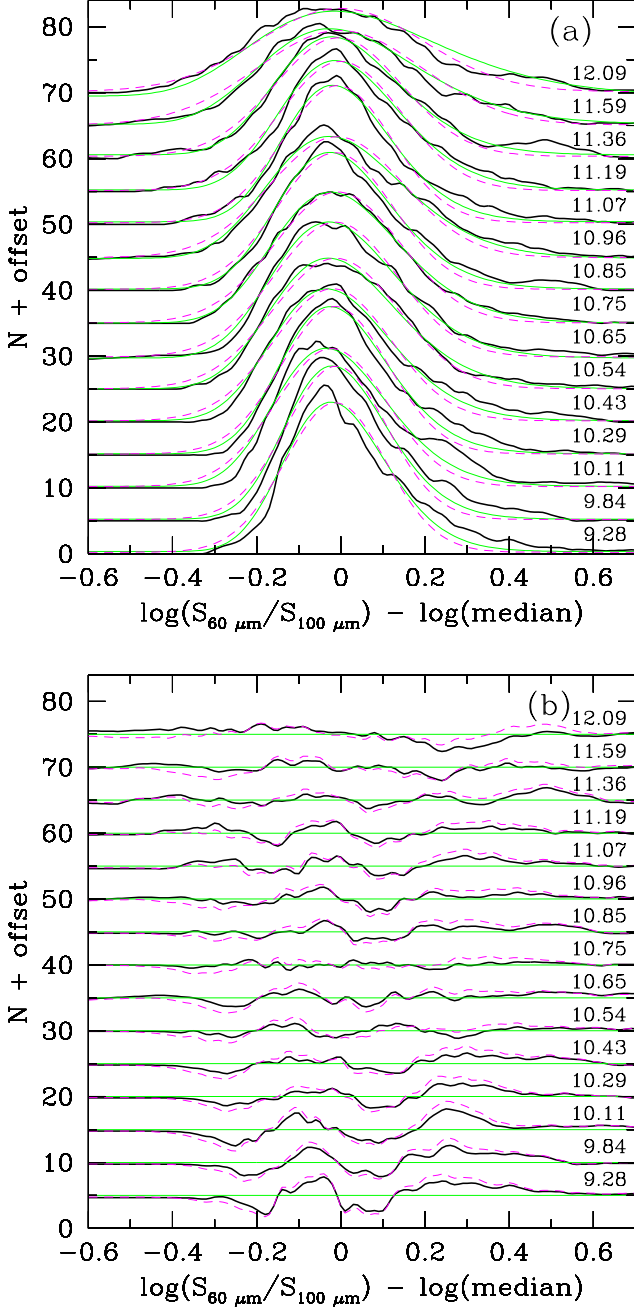


FIG. 4.— **upper panel:** The $\mathcal{R}(60, 100)$ distribution (heavy solid lines) with log normal fits (light green lines) and linear Gaussian fits (light dashed magenta lines). Offsets for each luminosity class are inserted as in Fig. 3. The median $\mathcal{R}(60, 100)$ has been removed for comparison of luminosities. **bottom panel:** The subtracted residuals are shown for both log normal (heavy line) and linear gaussian fits (dashed light line). Note that an improved fit, in the sense of reduced χ^2 cannot be obtained by a first order term of the form x^*G . A higher order term is required to obtain a better fit, which is not justified for the present data set.

The results of our fitting are shown in Fig. 4a, with each luminosity bin of the color histogram offset for clarity. The median has been removed from each histogram in order to compare directly the form of the distributions at various values of L_{TIR} . Fits of log normal distribution (light green line) and linear gaussian (light dashed magenta line) are shown. The residuals are plotted in Fig. 4b, emphasizing the superior fit of the log normal, as well as the skewed nature of the distribution. Heavy lines show the residuals from a log gaussian fit, while the light

dashed magenta lines show the residuals from a linear gaussian fit. While the skew is an apparently large and systematic effect, (it appears as a double-S, integral shape) the most significant deviations occur in the wings of the distribution, where our error bars are larger than the skew due to the rapidly diminishing number of sources in each histogram bin. For completeness we attempted to fit the skewed component with a multiplicative factor $x \times \exp[-z^2/2]$, but that did not improve the χ^2 . The systematic skew to the distribution therefore cannot be removed without a term which is too high an order to justify from the statistics of the sample. We therefore use the log-normal distribution fit as the best representation of the 1.2Jy IRAS galaxy sample. Note also that the residual skew is negligible near the intermediate luminosity bins of the population (the best sampled region) and becomes more pronounced towards the luminosity extremes. The skew may therefore partially be a result of including broader luminosity ranges in the distribution to retain equal number bins.

The distribution over $\mathcal{R}(60, 100)$ color can then be expressed as

$$\mathcal{G}(C) = \exp(-1/2 \times [(C - C_i)/\sigma_C]^2),$$

where $\sigma_C = 0.065$, $C = \log \mathcal{R}(60/100)$,

$$C_i = C_* \times \left(1 + \frac{\mathcal{L}_*}{L_{\text{TIR}}}\right)^{-\delta} \times \left(1 + \frac{L_{\text{TIR}}}{\mathcal{L}_*}\right)^{\gamma}$$

with, $\gamma = 0.16$, $\delta = 0.02$, $C_* = 0.45$, $\mathcal{L}_* = 5.0 \times 10^{10} L_{\odot}$

As the residual skew is close to symmetrical about the gaussian fit peak, we find that our fit to the distribution describes nearly the same function as the median and first/last quartile expression (a log-normal) presented in the previous section. The formal $\Phi(\mathcal{L}, C)$ is then expressed as follows, where we have derived the TIR luminosity function directly from the 1.2Jy catalog as described in the previous section,

$$\begin{aligned} \Phi(\mathcal{L}, C) d\mathcal{L} dC &= \Phi_1(\mathcal{L}) \times \Phi_2(C) d\mathcal{L} dC \\ &= \rho_* \times \frac{\mathcal{L}^{(1-\alpha)}}{\mathcal{L}_*} \times \left(1 + \frac{\mathcal{L}}{\mathcal{L}_*}\right)^{-\beta} \times \exp[-1/2 \left(\frac{C - C_i}{\sigma_C}\right)^2] d\mathcal{L} dC, \end{aligned}$$

with $\mathcal{L} = L_{\text{TIR}}$, $\rho_* = 4.34 \text{ Mpc}^{-3} L_{\odot}^{-1}$, $\mathcal{L}_* = 10^{10.7} L_{\odot}$, $\alpha = 1.55$, $\beta = 2.10$,

$$C = \log(S_{60\mu\text{m}}/S_{100\mu\text{m}}), C_i \text{ as above, } \sigma_C = 0.065.$$

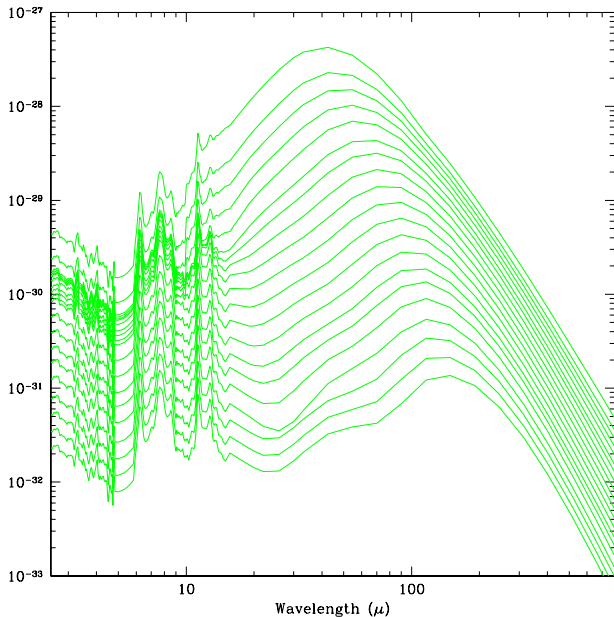


FIG. 5.— The range of local SEDs used in our model from the catalog of Dale et al. (2001, 2002). The flux units are $\text{ergs/s/cm}^2/\text{Hz}$ normalized to the median luminosity of a $z = 0.1$ galaxy in our model.

Our analysis has suggested that the $\mathcal{L}-\mathcal{C}$ distribution is best described with a dual power-law in \mathcal{L} with a break luminosity $5.0 \times 10^{10} L_{\odot}$, a faint end slope of $\delta = 0.02$ and a bright end slope of $\gamma = 0.16$. We offer two possible physical interpretations of this result.

Firstly, this may be the point of transition from cirrus-dominated luminosity to active star formation (i.e. high-density photo-dissociation regions, etc.) dominating the luminosity. The different power laws then arise because in the former case the luminosity increases mostly by making the emitting dust mass larger, whereas for active star formation, the heating drives the luminosity.

Secondly, this may be the point of transition from where the $60 \mu\text{m}$ band still has fluctuating grain emission contributing, to having the $60 \mu\text{m}$ band dominated by large dust grains. Once large dust grains dominate the $60 \mu\text{m}$ flux, the $\mathcal{R}(60, 100)$ ratio begins to look like a black-body ratio, leading naturally to the broken power-law relation. However in this case, the high luminosity, steep portion of the relation should scale with dust temperature like $\mathcal{L} \propto T^5$. Since this is not observed, this second explanation cannot dominate the observed relation.

4. CONSEQUENCES OF THE $\mathcal{L}-\mathcal{C}$ RELATION FOR EVOLUTION MODELS

Several authors have recently modeled the evolution of dusty galaxies using pure, or nearly pure, luminosity evolution, reproducing the observed counts and backgrounds at IR through sub-mm wavelengths (e.g. Blain et al. 1999a,b; Malkan & Stecker 2000; Rowan-Robinson 2001; Chary & Elbaz 2001; Chapman et al. 2002b; Franceschini et al. 2001). None of these models include a bi-variate luminosity function (LF), and at best map the dust temperature or spectral shape monotonically to the luminosity.

The spectral shape of the far-infrared background (FIRB) detected by *DIRE* at 140 and 240 μm (Puget et al. 1996; Fixsen et al. 1998) indicates a peak at $\sim 200 \mu\text{m}$. However, the width

of the peak suggests that galaxies over a large range in redshifts and/or dust temperature contribute to the FIRB. There is a degeneracy of dust temperature with redshift (Blain 1999), since both translating a source to higher redshift and decreasing the dust temperature will shift the SED to lower frequency. This suggests an urgency to explore the effect of the bi-variate LF on evolutionary models.

4.1. A color added evolution model

Our goal is to understand the key differences in $\Phi(\mathcal{L}, \mathcal{C})$ from the single variable $\Phi(\mathcal{L})$. We turn to Monte Carlo simulations of a pure luminosity evolution paradigm, similar to the models of the above authors. In companion papers (Lewis et al. 2003, S. Chapman in preparation), we demonstrate that our model is able to simultaneously fit the farIR background and the counts at various wavelength bands.

We evolve the local FIR luminosity function (LF) using $\Phi(L, \nu) = \Phi_0(L/g(z), \nu_0(1+z))$. Our evolution function follows a power law in redshift, $g(z) = (1+z)^4$, out to $z=2.6$. Beyond $z=2.6$ the function drops again as $g(z) = (1+z)^{-4}$ to avoid over-predicting the farIR background. This power-law index is chosen based on evolutionary models fit to both optical and sub-mm wavelength data (Blain et al. 1999a,b). The evolution to $z = 2.6$ was chosen as this provided the best fit to the joint radio/sub-mm sample of galaxies (Chapman, Lewis & Helou 2002, Lewis et al. 2003) – currently the best constraint on high- z farIR galaxy evolution (Blain et al. 1999a). The redshift $z = 2.6$ is also close to the consensus of the median redshift for SCUBA sources suggested for example by photometric redshifts in Ivison et al. (2002). In order to match the pure luminosity evolution, we truncate the evolved functions at low luminosity and at both extremes of color, so that they integrate to identical numbers of sources per comoving volume.

One additional assumption in this model is that the bi-variate distribution, $\Phi(\mathcal{L}, \mathcal{C})$, evolves in \mathcal{L} as a function of redshift, while the relation as observed locally between \mathcal{L} and \mathcal{C} holds at all redshifts. The width of the distribution in \mathcal{C} follows our measured relation from section 3, which remains close to constant in $\log(\mathcal{R}(60, 100))$. This implies that the characteristic dust temperature of higher redshift sources will be greater because of the rise in \mathcal{L} .

We note however, that while the no evolution hypothesis for \mathcal{C} is the simplest, it is not necessarily the obvious choice physically. Higher redshift sources may have distinctly different dust properties than local analogs. For instance, metallicities will likely be lower, there may be less dust to heat, and dust may be less centrally concentrated. This form of evolution might lead to the $\mathcal{R}(60, 100)$ distribution being biased to cooler IR colors with increasing redshift. In the absence of any strong constraint from the counts or background (Lewis et al. 2003, S. Chapman in preparation), this assumption needs to be tested by future observational data sets. However, we shall examine in the following section the preliminary evidence in support of this simple hypothesis.

We then incorporate this hypothesis into our Monte Carlo models, drawing $\mathcal{R}(60, 100)$ values from the evolving $\Phi(\mathcal{L}, \mathcal{C})$ to fill our desired survey volume. This model does not include observational error, but should accurately represent the chance of observing a source with a given IR color in a particular survey. The simulation is cut off at $10^8 L_{\odot}$ in order to avoid truncation effects from the fixed comoving number density in the luminosity functions.

In order to tie our evolving $\mathcal{L}(\text{TIR})$ luminosity function to ob-

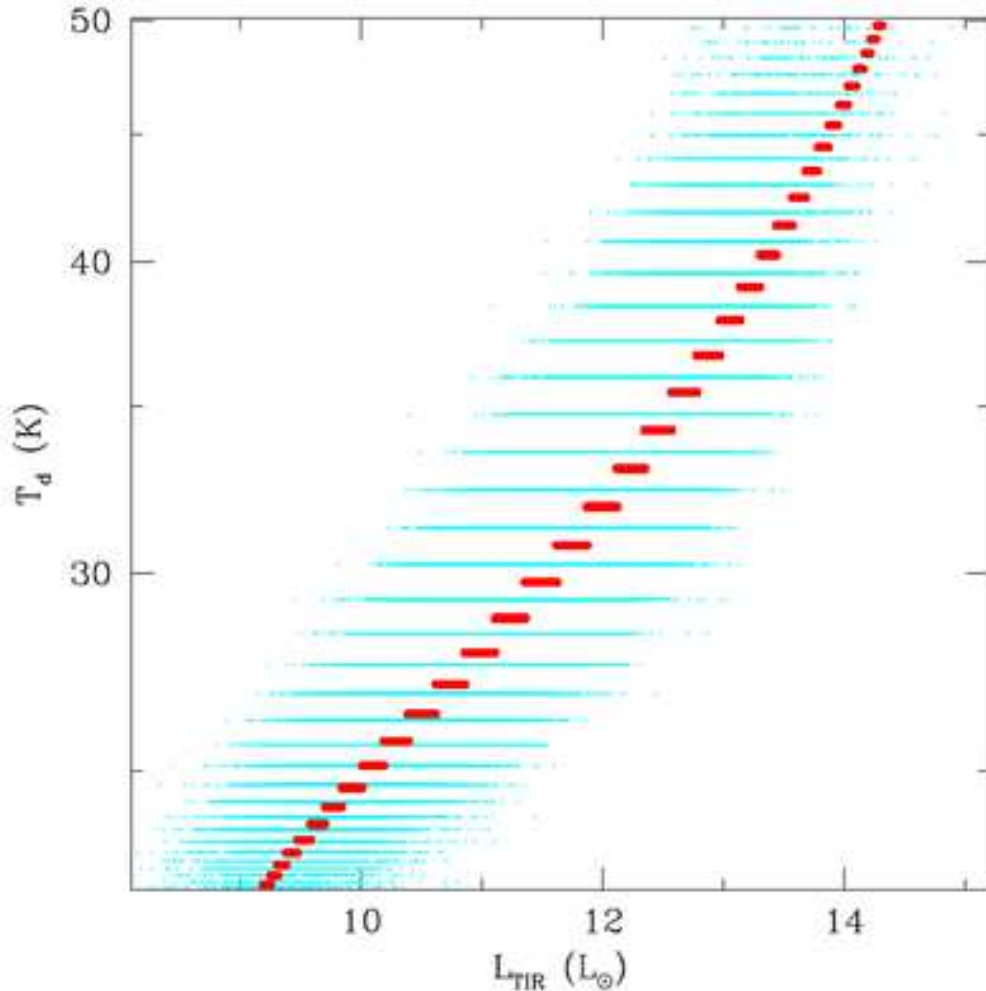


FIG. 6.— A plot of the L - T_d plane showing points drawn from our Monte Carlo sampling of the evolving bi-variate LF, and depicting all objects in the simulated volume of the survey regardless of their detectability by various instruments. For comparison we show a representation of the same evolving model with a very narrow range of colors for each luminosity (bold, offset points). The abscissa has been mapped from $\mathcal{R}(60, 100)$ to dust temperature (T_d) using the single temperature greybody which provides the best fit to the SED template. The quantized appearance of the points in T_d results from the individual 64 SED classes considered. The LF with narrow range of IR color closely approximates a single variable LF whereby luminosity maps monotonically to T_d or IR color.

servable quantities, we map each galaxy with a given L_{TIR} and $\mathcal{R}(60, 100)$ value to a spectral energy distribution (SED) shape. Normalization of the SEDs is accomplished by integrating the SED over the 3–1100 μm range and scaling to the adopted L_{TIR} . Spectral templates are taken from the Dale et al. (2001, 2002) catalog, divided into 64 classes from $\mathcal{R}(60, 100)=0.29$ to 1.64, corresponding roughly to single component dust temperature models of 19 K to 56 K. Representative SEDs from our catalog are shown in Fig. 7. The global galaxy SEDs adopted here use a power-law distribution of dust over heating intensity \mathcal{U} in order to reproduce the range of photometric and spectroscopic properties observed by IRAS and ISO for galaxies in the local Universe. Dale & Helou (2002) specifically investigate the dust emissivity of the local IRAS galaxies, using the sub-mm data presented in Dunne et al. (2000). They find the dust emissivity should vary with environment with $\beta = 2.5 - 0.4 \log \mathcal{U}$, where \mathcal{U} is the local radiation field.

4.2. Model Results and Implications

To underscore the effect of not including the $\Phi(\mathcal{L}, \mathcal{C})$ distribution in the redshift evolution, we show in Figs. 6–8 the out-

put from our luminosity evolution models, with and without the broad local color distribution in the LF.

In Fig. 6, we plot the \mathcal{L} - T_d plane showing points drawn from our Monte Carlo sampling of the evolving bi-variate LF. We compare directly the bi-variate $\Phi(\mathcal{L}, \mathcal{C})$ to an equivalent $\Phi(\mathcal{L})$, with a very narrow range of colors for each luminosity (bold, offset points). The ordinate has been mapped from $\mathcal{R}(60, 100)$ to dust temperature (T_d) using the single temperature greybody which provides the best fit to the SED template. The quantized appearance of the points in T_d results from the individual 64 template SED classes considered. The LF with narrow range of IR color closely approximates a single variable LF whereby luminosity maps monotonically to T_d or IR color. Fig. 6 provides an overview of $\mathcal{R}(60, 100)$ as a function of \mathcal{L} , simply extrapolating the local $\mathcal{L}-\mathcal{C}$ relation to the required luminosities – our baseline assumption in this model. The distribution is symmetric in $\log(T_d)$ about each luminosity. As the $\Phi(\mathcal{L}, \mathcal{C})$ distribution remains identical to our locally characterized form (§ 3) for all redshifts, any deviations from the median local relation reflect only the scatter in the relatively small numbers of luminous galaxies in this simulated survey volume.

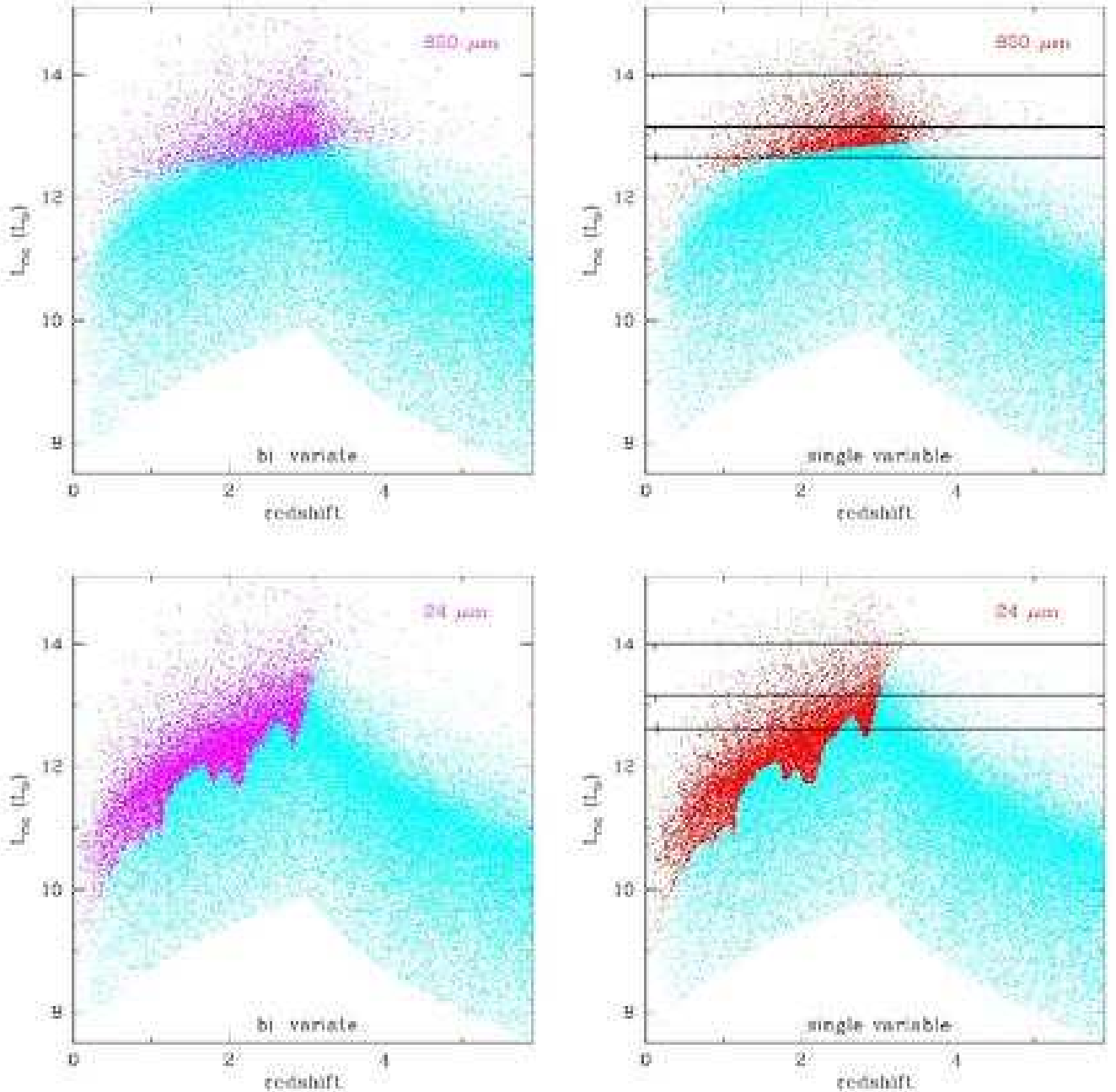


FIG. 7.— Comparison of our Monte Carlo representation of the evolving $\Phi(\mathcal{L}, \mathcal{C})$ to an evolving model LF with a one-to-one mapping of luminosity to color. The lighter symbols represent only luminosity and thus follow identical distributions in both cases. The difference between models is apparent when flux limited surveys are defined on the model points. We overlay flux limited samplings of the model points at $24\mu\text{m}$ and $850\mu\text{m}$ with darker symbols. Structure in the $24\mu\text{m}$ survey is a result of PAH bands (rest $\sim 10\mu\text{m}$) being redshifted through the SIRTf $24\mu\text{m}$ filter. In the single variable LF model, luminosities map uniquely to fluxes and lines can be drawn which reflect fixed temperatures, shown at 50 K, 38 K and 35 K, top to bottom.

In Fig. 7, we show the L_{TIR} distribution as a function of redshift. The left panels show the $\Phi(\mathcal{L}, \mathcal{C})$ model, while the right panels show the single variable LF model. Until we apply a flux limit to the figure (darker points), there is no difference between the visualizations since they have the same luminosity evolution formalism. Fig. 7 is our Monte Carlo representation of the evolving LF; vertical slices reveal the dual power law $\Phi(\mathcal{L})$ at each redshift. Note that with comoving number density, in the absence of luminosity evolution, a local physical density of N objects per Mpc^3 corresponds to a physical density of $N * (1+z)^3$ at redshift z . In this type of model the evolution is not

necessarily meant to imply that ULIRGs fade into less luminous LIRGs with time. Instead, it provides a picture where, for instance, the local counterparts with volume densities similar to ULIRGs at $z \sim 1$ have $10^{11.5} L_{\odot}$ at the present-day. This form of evolution is then *not* describing the internal physics of the IR luminous population; high- z ULIRGs do not evolve into similar local ULIRGs, but instead likely form ellipticals (e.g., Sanders & Mirabel 1996; Tacconi et al. 2002), fading away from the LF.

When flux limited surveys are considered in the context of Fig. 7 ($850\mu\text{m}$ – top, $24\mu\text{m}$ – bottom), differences in the two models become manifest. In the case of the single variable dis-

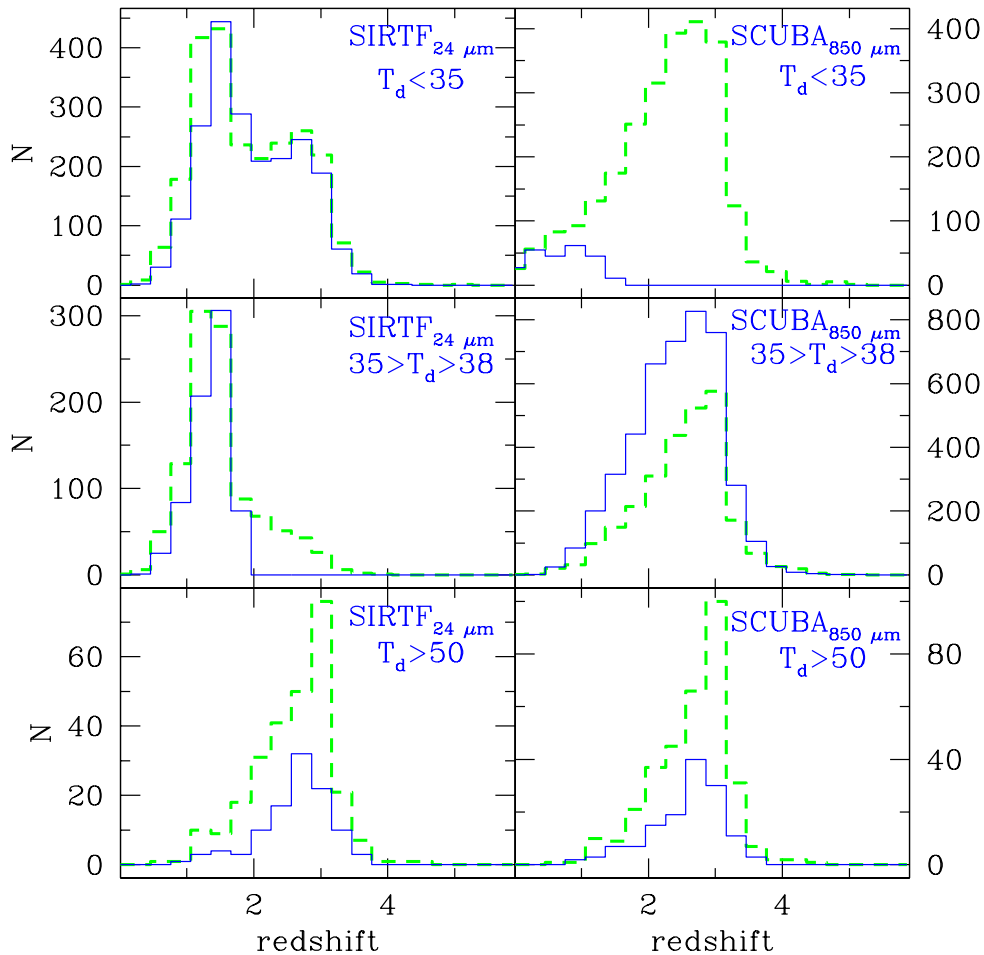


FIG. 8.— Histograms of sources with redshift are plotted for the cold, medium and hot range in IR color (again mapped to the equivalent single component dust temperature). Heavy dashed lines represent the evolving $\Phi(\mathcal{L}, \mathcal{C})$ distribution, while lighter solid lines represent the single variable LF. An excess of hotter sources by a factor >2 is revealed for the $\Phi(\mathcal{L}, \mathcal{C})$ model where all sources are luminous enough to be detected regardless of the observing band. For the medium and cold temperature slices, the effective luminosity ranges lie near the sensitivity limits of the survey which additionally affect the histograms.

tribution, each L_{TIR} point maps uniquely to a flux for a given wavelength. However in the bi-variate LF, each L_{TIR} point corresponds to a probability distribution of fluxes corresponding to the log-normal distribution in $\mathcal{R}(60, 100)$ and the associated range of SED templates that can be tied to the L_{TIR} value. The sensitivity limits in the $850\ \mu\text{m}$ and $24\ \mu\text{m}$ bands are shown for characteristic survey depths with SCUBA and SIRTIF (2 mJy r.m.s., and 0.1 mJy r.m.s., respectively). The structure in the $24\ \mu\text{m}$ survey is a result of PAH bands (rest $\sim 10\ \mu\text{m}$) being redshifted through the SIRTIF $24\ \mu\text{m}$ filter. At $850\ \mu\text{m}$, the K-correction from the rising grey-body dust SED results in a flat Luminosity-Flux relation for redshifts $z \gtrsim 1$.

The effect is subtle in Fig. 7, as both the luminosity function and the color distribution are scattering the observed fluxes, largely canceling dramatic differences in the effective luminosity limits probed with redshift. However, the most important difference between the bi-variate and luminosity-only models is apparent in Fig. 7: in the simpler $\Phi(\mathcal{L})$ model, the flux limit for a given wavelength translates at each redshift into a transition range of luminosities, within which galaxies are or are not detected depending on their color. We draw lines on the single variable model for \mathcal{L} corresponding to T_d of 35 K, 38 K, and

50 K, using the mapping illustrated in Fig. 6.

The implications of this model difference are therefore much more apparent in a direct analysis of T_d , as demonstrated in Fig. 8. Histograms of sources versus redshift are plotted for the $850\ \mu\text{m}$ and $24\ \mu\text{m}$ bands, comparing the detectability of hotter and cooler IR colors (again mapped to the equivalent single component dust temperature). Heavy dashed lines represent the evolving $\Phi(\mathcal{L}, \mathcal{C})$ distribution, while lighter lines represent our approximation to a single variable LF.

We first consider the model differences for a SCUBA $850\ \mu\text{m}$ survey in Fig. 8. A cut for detectable sources colder than $T_d < 35\ \text{K}$ (shown in Fig. 7) lies along the sensitivity limit of SCUBA. This results in the most dramatic difference between the models, since in the bi-variate model, the steep luminosity function scatters many more cold, under-luminous sources into the sample than the corresponding loss of hotter, higher luminosity sources. The selection along the cold side of the grey-body peak for SCUBA therefore produces a substantial population of cold sources which are strikingly absent when only the single variable LF is included in the evolution. This difference results in an important prediction of the existence of cold and luminous galaxies at moderate to high redshifts – a predic-

tion which has been verified through the detection of ULIRGs with $T_d < 30$ K (Chapman et al. 2002a). The opposite effect is shown in the middle panel of Fig. 8 for the range $35 < T_d < 38$ K, producing a band in luminosity lying just above the sensitivity limit of our SCUBA survey in Fig. 7. The bi-variate model now scatters the warmer sources below our detection limit, resulting in a dearth of sources relative to the single variable LF. For the hottest sources ($T_d > 50$ K), the luminosities are large enough (Fig. 7) that the sensitivity limit of the survey has no bearing on the observed sources, and the comparison of models simply reflects the steep luminosity function which asymmetrically scatters more low luminosity hot sources into the temperature cut than luminous cold sources which fall beneath the cut. The bi-variate $\Phi(\mathcal{L}, \mathcal{C})$ model thus predicts almost twice as many warm galaxy detections, even though the underlying luminosity distribution is the same as in the $\Phi(\mathcal{L})$ model.

For surveys selecting sources along the hot dust side of the grey-body peak, that being the case for all the accessible wavelengths of SIRTf except $170\ \mu\text{m}$, colder luminous sources will be missed and hotter low luminosity sources will be preferentially detected. This is exactly in the opposite sense to the situation for sub-mm selected surveys (such as with SCUBA), preferentially detecting colder sources at a given luminosity (Eales et al. 1999, Blain et al. 2002).

The sensitivity limit of SIRTf is adversely affected by the steep Wien slope of the far-mid-infrared SED, making more distant sources difficult to detect and resulting in the steep sensitivity curve in Fig. 7. The result in Fig. 8 is that the histograms near the sensitivity limit of SIRTf will be dominated by the large numbers of sources lying both above and below any fixed temperature cut. The histograms in the cold and warm $24\ \mu\text{m}$ panels therefore continue to show the asymmetric *shuffling* of sources due to the steep luminosity function, but only as a small perturbation on the large number of sources which are unaffected by the sensitivity limit. However, for hotter dust temperatures, an excess of a factor greater than two of sources is predicted by the $\Phi(\mathcal{L}, \mathcal{C})$ model. This excess occurs for the SIRTf $24\ \mu\text{m}$ band for the same reason discussed above for SCUBA. All sources are luminous enough to be detected regardless of their temperature, and there are far more lower luminosity sources which are boosted by the bi-variate LF into the $T_d > 50$ K bin than vice versa.

Consideration of the model differences in Fig. 8 also addresses the question of the SCUBA/SIRTf galaxy overlap. As the SCUBA and SIRTf observing windows lie on opposite sides of the dust spectral energy peak, the direct overlap of the populations is a strong function of the dominant dust temperature. In particular, a cold ($T_d < 30$ K) SCUBA population may be difficult to detect even in the deepest SIRTf exposures, as revealed in the high redshift excess of cold SCUBA sources compared with the SIRTf population. Scrutiny of Fig. 7 along the survey flux limits reveals that at $z \lesssim 3$, the individual SCUBA galaxies detected in either model are mostly detected by SIRTf at $24\ \mu\text{m}$ at this survey depth. However, deeper sub-mm surveys by instruments like the *Large Millimeter Telescope* (Hughes et al. 2001) may uncover fainter cold galaxies at lower redshifts which would require very deep SIRTf exposures to detect. By contrast, most or all of the SCUBA sources should be detected by SIRTf over all redshifts when the characteristic dust temperatures are higher, as suggested by the similar $N(z)$ in the lower panels of Fig. 8.

Figs. 7&8 are also suggestive of the effect of the evolutionary form on the detectability of galaxies at different wavelengths.

The properties of the sources detectable at high redshift are a sensitive function of the evolutionary form adopted – in our scenario, lower redshift peaks in the evolution function would result in an appreciably smaller fraction of high redshift galaxies detected (effectively generating differences in the redshift distributions). For example, a direct application of our $\Phi(\mathcal{L}, \mathcal{C})$ model to the SCUBA population (Chapman, Lewis & Helou 2002, Lewis et al. 2003) has suggested a best fit peak at a lower redshift of $z \sim 2.5$. However, this is extremely sensitive to any evolution in the IR color distribution (but see § 5 to follow). We defer detailed fitting of our model to the available high redshift counts and FIRB to a companion paper (Lewis et al. 2003). Ultimately, redshift surveys of SIRTf and SCUBA galaxies will be required to test the detailed form of the evolution function (see Chapman et al. 2003a for preliminary results on the SCUBA galaxy redshift distribution).

5. COMPARISON WITH DATA OUT TO HIGHER REDSHIFTS

Our comparison of evolving a single variable LF versus a bi-variate $\Phi(\mathcal{L}, \mathcal{C})$ (Figs. 6–8) clearly demonstrates that an over-simplified representation of the galaxy population can miss large classes of detectable sources at high redshifts. It is then crucial to understand whether the IR color distribution itself has evolved with redshift.

While much attention has been paid to the luminosity evolution of ULIRGs (e.g. Blain et al. 1999a,b; Chary & Elbaz 2001; Malkan & Stecker 2001; Rowan-Robinson 2001; Chapman et al. 2002b; Ivison et al. 2002), there has been no study of the $\mathcal{R}(60, 100)$ evolution. The simplest scenario, which we considered above, is that the $\mathcal{R}(60, 100)$ correlation with L_{TIR} continues to higher luminosities, extrapolating the expressions derived in this work for the local $\mathcal{R}(60, 100)$ distribution.

Existing data sets are largely inadequate for characterization of the high- z IR color distribution. ISOPHOT and SCUBA galaxies do not generally have accurate redshifts or even detections at sufficient wavelengths to measure the rest frame $\mathcal{R}(60, 100)$. However, a survey of moderate redshift, luminous IRAS galaxies (Stanford et al. 2000) provides an initial foray into the higher redshift $\mathcal{R}(60, 100)$ distribution (for a complementary analysis of this population, see also Blain, Barnard & Chapman 2003). This section will focus on the Stanford et al. IRAS galaxies, as well as the microjansky radio sources (Chapman et al. 2003b) to assess our $\Phi(\mathcal{L}, \mathcal{C})$ characterization.

5.1. $60\ \mu\text{m}$ -selected LIRGs/ULIRGs at $0.1 < z < 0.9$

A recent sample of distant LIRGs and ULIRGs from Stanford et al. (2000) has an effective sensitivity only 2–3 times higher than that of the deepest ISOPHOT $170\ \mu\text{m}$ surveys, and we can use this sample to study the higher redshift $\Phi(\mathcal{L}, \mathcal{C})$. The Stanford et al. sample was selected from a positional cross-correlation of the IRAS Faint Source Catalog with the FIRST database. Objects from this set were selected for spectroscopy by virtue of following the well-known star-forming galaxy correlation between 1.4 GHz and $60\ \mu\text{m}$ flux, and by being optically faint on the POSS. Optical identification and spectroscopy were obtained for 108 targets at the Lick Observatory 3 m tele-

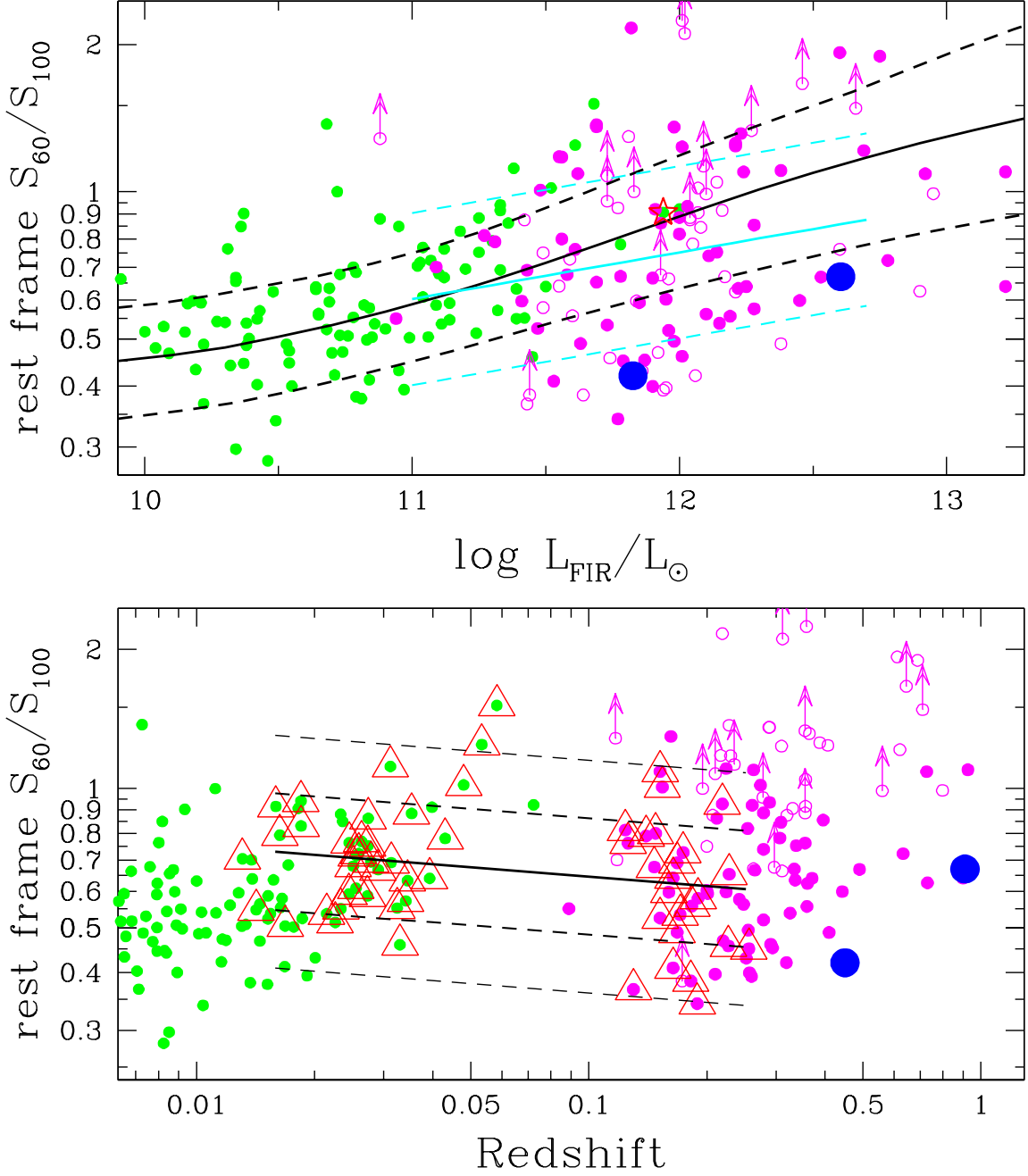


FIG. 9.— **upper panel:** The dependence of rest frame $\mathcal{R}(60, 100)$ (roughly dust temperature) on L_{FIR} is shown. LIRGs and ULIRGs from the Stanford et al. (2000) FIRST/60 μm selected sample, with redshifts from 0.1 to 0.9 (magenta circles), appear as a consistent extension to local IRAS-BGS galaxies (green circles). Many Stanford et al. sources are detected at 60 and 100 μm (solid circles), although some have only tentative 100 μm measurements when analysed in XSCANPI (open circles); those without 100 μm detections at all are shown as limits. The fit to the Stanford et al. sources between $11.5 < \log L_{\text{FIR}} < 12.5$ is shown with lighter solid and dashed lines, for the $\pm 1\sigma$ envelope. Two FIRBACK 170 μm selected galaxies from Chapman et al. (2002a) are shown as large circles. Our best fit correlation from section 3 and 1σ deviations are overlaid as the thick solid and dashed lines. Arp220, the ULIRG typically used for comparison with high- z luminous galaxies, is identified with a star. **lower panel:** The $\mathcal{R}(60, 100)$ ratio is shown as a function of redshift for the same sources. Overlapping luminosity regions can be compared directly. Triangles have $\log L_{\text{FIR}} \sim 11.5 \pm 0.5$. Fits to the population overlapping in luminosity at $L_{\text{TIR}} = 3 \times 10^{11} L_{\odot}$ signalled by oversized triangles, is shown with a solid line, along with $1\sigma, 2\sigma$ distributions as dashed lines. The slopes of the fit line is not significantly different from zero.

scope. Most objects show spectra typical of starburst galaxies, and do not show the high ionization lines of active galactic nuclei. The redshift distribution covers $0.1 < z < 0.9$, with 13 objects at $z > 0.5$ and an average redshift of $\bar{z} = 0.31$.

5.1.1. The dependence of $\mathcal{R}(60, 100)$ on \mathcal{L}

We first address the issue of the dependence of width in \mathcal{C} ($= \mathcal{R}(60, 100)$) on the luminosity. Fig. 9a shows the $\mathcal{R}(60, 100)$ versus L distribution of the Stanford et al. sample relative to

our fit \mathcal{C} relation from section 3, overlaying the local BGS IRAS galaxies observed with SCUBA by Dunne et al. (2000) for reference. The rest frame $\mathcal{R}(60, 100)$ has been calculated by fitting the Dale et al. (2001, 2002) template SEDs to the observed frame 60 μm , 100 μm , and radio points, and extracting the restframe 60 μm , 100 μm fluxes. The moderate- z sources from Stanford et al. (2000) are not, however, all detected at 100 μm . We have run the IPAC application **XSCANPI** over all

103 Stanford sources to derive improved estimates of the 60 and $100\ \mu\text{m}$ fluxes, finding 46 with spurious $100\ \mu\text{m}$ measurements. The sources without $100\ \mu\text{m}$ detections are presented as lower limits to $\mathcal{R}(60, 100)$, while those with only marginal $100\ \mu\text{m}$ detections are differentiated with open symbols. The fits to the distribution are then derived, using only sources with secure $100\ \mu\text{m}$ detections. The fit result is shown as the lighter solid line with the $\pm 1\sigma$ lines shown as lighter dashed lines in the upper panel of Fig. 9. The sources with $100\ \mu\text{m}$ limits appear to be uniformly distributed amongst the $100\ \mu\text{m}$ detected sources, and a large systematic skew is unlikely.

The median relation between L_{FIR} and $\mathcal{R}(60, 100)$ is similar to that observed locally, although it falls to the -1σ deviation of the local relation for the most luminous Stanford sources. However, these most luminous sources are not very numerous and contribute negligibly to the fit lines. Moreover, the fit did not take into account the lower limits to $\mathcal{R}(60, 100)$. The median of this luminous tail of Stanford sources on their own is in fact more consistent with the local relation.

The width of the Stanford distribution matches the extrapolation from the $1.2\ \text{Jy}$ envelope at $L_{\text{FIR}} = 3.1 \times 10^{12} L_{\odot}$ (Fig. 9a). However, the width of the Stanford sources exceed the local distribution by a factor of $\sim 50\%$ at $L_{\text{FIR}} = 4.6 \times 10^{11} L_{\odot}$, and there is an apparent excess of LIRG/ULIRG class sources as cold as the two FIRBACK galaxies discussed in the introduction, FB1-40 and FB1-64 at their respective FIR luminosities (see § 5.1.3). As the Stanford et al. sources were selected in the $60\ \mu\text{m}$ band, a direct comparison with our $1.2\ \text{Jy}$ catalog is justified, with the assumption that the fainter flux limits of the Stanford et al. sample simply allows a probe of the higher luminosity distribution out to moderate redshifts where evolution is still not likely to be a large effect. However, even for sources with detected $100\ \mu\text{m}$ fluxes, the signal-to-noise ratio is not high, and photometric scatter may affect the width of the diagram. A further complication is that while the rest-frame $\mathcal{R}(60, 100)$ has been demonstrated to correlate well with cold dust temperature using $850\ \mu\text{m}$ measurements (Dunne et al. 2000), the observed $\mathcal{R}(60, 100)$ becomes less effective at constraining the cold temperature properties as redshifts increase beyond $z \sim 0.5$. The majority of the Stanford sources are at $z \lesssim 0.4$ and this should not result in a large effect on the average sample properties. Observations at $850\ \mu\text{m}$ will be required to properly assess the contribution of the Stanford sources at higher redshifts to the width of the distribution.

We therefore conclude that the direct extrapolation from the local IRAS galaxies is consistent with the width of the Stanford et al. sources, with a possibility of an increasing width at lower luminosities in the Stanford sample. We note, however, that the width of even the local distribution at the highest luminosities is highly uncertain, and a change in the slope of the broadening function could be in agreement to within the errors.

5.1.2. The dependence of $\mathcal{R}(60, 100)$ on redshift

We now address the possible evolution in the $(\mathcal{L}, \mathcal{C})$ relation with redshift. In Fig. 9b, the $\mathcal{R}(60, 100)$ ratio is shown as a function of redshift for the same sources. The overlapping luminosity regions can be compared directly. Triangles have $\log L_{\text{FIR}}/L_{\odot} \sim 11.5 \pm 0.5$, in both IRAS-BGS and Stanford et al. galaxies. A fit to the overlapping luminosity populations (signalled by oversize symbols) is shown with a solid line, along with 1σ and 2σ envelopes.

The salient point of Fig. 9b is that the Stanford sources do not appear significantly different in the median than the local com-

parison sample. The large fraction of Stanford sources with lower limits and uncertain $100\ \mu\text{m}$ fluxes may be responsible for the median point lying somewhat lower than local galaxies. The current data therefore do not support a scenario in which the median $\mathcal{R}(60, 100)$ in \mathcal{C} varies significantly with redshift out to $z \sim 1$. The width in \mathcal{C} of both luminosity bins is similar in Fig. 9b, and wider than the local distribution. This is consistent with the broadening of \mathcal{C} with luminosity, and suggests that the redshift evolution affects the width in \mathcal{C} only in so far as higher redshift sources have characteristically higher L . However, the statistics for sources with $z > 0.5$ are poor. With identified redshifts for increased numbers of sub-mm galaxies (see Chapman et al. 2003a), this issue will be directly addressable.

5.1.3. ISOPHOT $170\ \mu\text{m}$ galaxies at intermediate redshift

Recently, Keck spectra and UKIRT high spatial resolution near-IR imagery for two of the proposed highest redshift sources from the FIRBACK-N1 $170\ \mu\text{m}$ survey were obtained (Chapman et al. 2002a). These authors found that the redshifts of counterparts to the $170\ \mu\text{m}$ sources confirm that both sources are ULIRGs, but that their redshifts are significantly lower than implied by fitting a typical ULIRG SED to their farIR/sub-mm/radio SEDs. This indicates that they have cooler dust temperatures, $T_d \sim 30\ \text{K}$, than the canonical ULIRG values ($T_d \sim 45\ \text{K}$). As previous models have failed to predict the existence of such cold and luminous sources, these two galaxies therefore confirm the importance of considering the full $\Phi(\mathcal{L}, \mathcal{C})$ in evolutionary models.

In Fig. 9, we overplot these 2 FIRBACK ULIRGs on the local IRAS BGS and the Stanford LIRG/ULIRG sample; FN1-40 and FN1-64 are cold objects, lying near the -2σ level below the local median relation. While FB1-40,64 appear as cold objects relative to the local distribution in $\Phi(\mathcal{L}, \mathcal{C})$, there is not yet enough followup to ISOPHOT sources to know if \mathcal{C} has substantially evolved out to $z \sim 1$. FN1-40,64 remain at the periphery of the distribution, but are certainly not such unusual objects when compared to similar redshift ULIRGs from the Stanford et al. sample.

5.2. The \mathcal{L} - \mathcal{C} relation for microjansky radio sources

In this subsection, we test the lower luminosity \mathcal{L} - \mathcal{C} relation out to $z \sim 0.6$ using a sample of radio galaxies with $20\ \text{cm}$ fluxes ranging from $30\ \mu\text{Jy}$ to $500\ \mu\text{Jy}$ from Chapman et al. (2003b). These radio sources were observed in the sub-mm, and all have spectroscopic redshifts ranging from $z=0.1-0.6$. From this information we can estimate T_d and L_{FIR} by assuming the FIR-radio correlation for star forming galaxies (Helou et al. 1985) and a synchrotron spectrum with an index of $\alpha = -0.8$ (Richards 2000). T_d is estimated by taking the SED template from Dale & Helou (2002) which has the appropriate temperature to fit the radio and sub-mm points at the fixed redshift of the source. Note that we are only indirectly testing the \mathcal{L} - \mathcal{C} relation with these galaxies (we are estimating both \mathcal{L} and \mathcal{C} through local empirical correlations), and we cannot deconvolve variations in the \mathcal{L} - \mathcal{C} relation from the FIR-radio correlation.

We then restrict the sample to those sources with $L_{\text{FIR}} < 10^{11} L_{\odot}$ as the spectroscopic incompleteness introduces a severe bias for more luminous (and typically optically fainter) galaxies (as discussed in Chapman et al. 2003b). This also reduces the radio-bright AGN contribution to the sample, which will have much larger apparent L_{FIR} calculated in this manner due to the AGN generated radio excess.

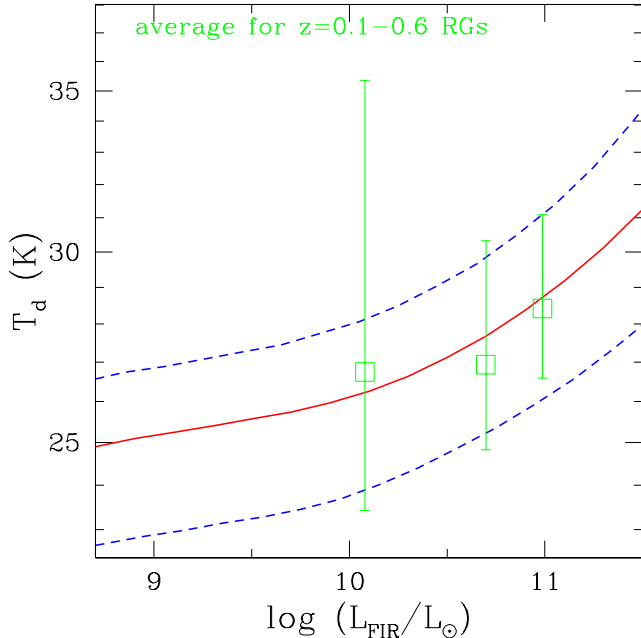


FIG. 10.— Dust temperature (T_d) versus the log of FIR luminosity for radio sources with $L_{\text{FIR}} < 10^{11} L_{\odot}$ and spectroscopic redshifts. Sources span $z = 0.1-0.6$, and have been divided into three equal number bins. The T_d and FIR values have been calculated from the redshift and the sub-mm/radio measurements as described in the text. Our derivation of the median and interquartile range of local IRAS galaxies from the 1.2 Jy catalog are shown. The agreement of the higher redshift sources with the local relation is remarkable.

In Fig. 10 we plot T_d versus FIR luminosity, along with our derived local IRAS galaxy relation from § 3. The average points in Fig. 10 do not include sources individually detected in the submillimeter, and the variance from measurement errors is expected to be comparable to that from scatter in the dust properties. Thus our points can only be used as a characterization of the average $\mathcal{L}-\mathcal{C}$ relation.

Fig. 10 demonstrates that the $L_{\text{FIR}} < 10^{11} L_{\odot}$ radio sources, spanning the redshift range $z = 0.1-0.6$ appear to follow the local IRAS color distribution very well. This suggests jointly that neither the $\mathcal{L}-\mathcal{C}$ relation nor the FIR-radio correlation can deviate significantly from local values for these sources. The analysis provides a direct consistency check of the lower luminosity tail of local IRAS galaxies with higher redshift star forming galaxies, of which the microjansky radio population should represent higher redshift specimens (e.g., Richards 2000).

CONCLUSIONS

We have analyzed the $\mathcal{R}(60, 100)$ distribution of local IR-luminous galaxies finding a best fit, low order analytical expression for the bi-variate luminosity function, $\Phi(\mathcal{L}, \mathcal{C})$. A log-normal distribution about a dual power law in the median $\mathcal{R}(60, 100)$ versus L_{TIR} is demonstrated to provide the best fit of the IRAS population over 4 orders of magnitude in L_{TIR} .

We then studied the redshift evolution of $\Phi(\mathcal{L}, \mathcal{C})$, using a luminosity evolution paradigm. We demonstrated that while similar luminosity regimes are detectable at $24 \mu\text{m}$ and $850 \mu\text{m}$, the dust temperatures represented by the detectable sources can differ by factors of > 2 . For a flux limited survey, the bi-variate $\Phi(\mathcal{L}, \mathcal{C})$ model predicts about twice as many warm galaxy detections as the equivalent single variable model, even though the underlying luminosity distributions are the same in the two models. In a similar manner, recently discovered populations of cold, luminous galaxies can be predicted naturally within our model. Consideration of the model differences also addresses the question of the SCUBA/SIRTF galaxy overlap, a strong function of the dominant dust temperature. A cold ($T_d < 30 \text{ K}$) SCUBA population may be difficult to detect even in the deepest SIRTF exposures, as revealed in the high redshift excess of cold SCUBA sources compared with the SIRTF population.

We compare our derived color relation with existing data for higher redshift IR galaxies. General agreement with the local color relation is found amongst all higher redshift galaxy populations considered. We therefore find no significant evidence for a variation in the median $\mathcal{R}(60, 100)$ ratio as a function of redshift.

We do find tentative evidence for a broadening of the IR color distribution at higher \mathcal{L} from both our local 1.2 Jy sample, and the moderate redshift high luminosity sample of Stanford et al. (2000). This suggests that redshift evolution does not in itself affect the width in \mathcal{C} . The baseline assumption that the locally measured $\mathcal{L}-\mathcal{C}$ relation holds over all redshifts is therefore a reasonable working hypothesis, to be verified with SIRTF data.

ACKNOWLEDGEMENTS

We thank Ian Smail and Andrew Blain for helpful discussions. An anonymous referee helped to improve the paper. GFL thanks the Australian Nuclear Science and Technology Organization (ANSTO) for financial support. This research has made use of the NASA IPAC Infrared Science Archive, which is operated by the Jet Propulsion Laboratory, California Institute of Technology, under contract with the National Aeronautics and Space Administration.

REFERENCES

- Alton, P.B., et al., 2000, *A&A*, 356 795
 Andreani, P., Franceschini, A., 1996, *MNRAS*, 283, 85
 Blain, A.W. 1999, *MNRAS*, 309, 955
 Blain, A.W., Smail, I., Ivison, R. J., & Kneib, J.-P. 1999a, *MNRAS*, 302, 632
 Blain, A.W., et al., 1999b, *MNRAS*, 309, 715
 Blain, A.W., Smail, I., Ivison, R., Kneib, J.-P., Frayer, D., 2002, in press at Physics Reports, (astro-ph/0202228)
 Blain, A.W., Barnard, V., Chapman, S.C., 2003, *MNRAS*, in press
 Chapman, S.C., Smail, I., Ivison, R., Helou, G., Dale, D., Lagache, G., 2002a, *ApJ*, 573, 66
 Chapman, S.C., Lewis, G., Scott, D., Borys, C., Richards, E., 2002b, *ApJ*, 570, 557
 Chapman, S.C., Lewis, G., Helou, G., 2002c, "A New Era in Cosmology", (ASP Conference Proceedings), eds. T. Shanks and N. Metcalfe, (astro-ph/0203095)
 Chapman, S.C., Blain, A., Ivison, R., Smail, I., 2003a, *Nature*, accepted
 Chapman, S.C., et al., 2003b, *ApJ*, in press, (astro-ph/0211075)
 Chary, R., Elbaz, D., 2001, *ApJ*, 548, 562
 Dale, D., Helou, G., Contursi, A., Silbermann, N.A., Kolhatkar, S. 2001, *ApJ*, 562, 142
 Dale, D., Helou, G., 2002, *ApJ*, 576, 159
 Dunne, L., et al. 2000, *MNRAS*, 315, 115
 Dunne, L., Eales, S. 2001, *MNRAS*, 327, 697
 Eales, S., et al., 1999, *ApJ*, 515, 518
 Eales, S., et al., 2000, *AJ*, 120, 2244
 Fisher, K., et al., 1995, *ApJS*, 100, 69
 Franceschini, A., et al., 2002, *ApJ*, in press, astro-ph/0111413
 Hughes, D. 2001, IGRAP International Conference on "Clustering at High Redshift", Marseilles (June 29 - July 2 1999), astro-ph/0003414
 Ivison, R., et al., 2002, *MNRAS*, in press, astro-ph/0206432
 Lewis, G., Chapman, S.C., Iyata, R., Irwin, M., Totten, E., 1998, *ApJL*, 505, 1
 Lewis, G., Chapman, S.C., Helou, G., Borys, C., Fahlman, G., Scott, D., 2003, *ApJ*, submitted.
 Lo, X., Gao, A., Guendl, P., 1997 *ApJ* 475, 103
 Malkan, M., Stecker, F.W., 2001, *ApJ*, 555, 641
 Reach, W.T., et al. 1995, *ApJ*, 451, 188
 Richards, E.A., 2000, *ApJ*, 513, 149
 Rowan-Robinson, M., 2001, *ApJ*, 549, 745
 Roussel, H., et al. 2003, *ApJ*, submitted

Sanders D. B. & Mirabel I. F. 1996, ARA&A, 34, 749

Smail, I., Ivison, R.J., Blain, A.W., 1997, ApJ 490, L5

Smail, I., Ivison, R.J., Blain, A.W., Kneib J.P. 2002, MNRAS, 331, 495

Soifer, T., Neugebauer, G., 1991, AJ, 101, 354

Stanford, A., Stern, D., van Breugel, W., De Breuck, C., 2000, ApJS, 131, 185

Tacconi, L., et al., 2002, A&A, in press